EasyChair Preprint
№ 11330

Performance Analysis of a Novel Single Flywheel Resettable-Inertia Damper

Delei Yu, Qigang Liang and Luyu Li

November 18, 2023

Performance Analysis of a Novel Single Flywheel Resettable-Inertia Damper

Delei Yu[1] Qigang Liang[2] Luyu Li[3]

[1]School of Civil Engineering, Dalian University of Technology, 2 Linggong Road, Ganjingzi District, Dalian 116024, Liaoning, China. Email:ydlengineer@163.com
[2]School of Civil Engineering, Dalian University of Technology, 2 Linggong Road, Ganjingzi District, Dalian 116024, Liaoning, China. Email: drqigang@gmail.com
[3]School of Civil Engineering, Dalian University of Technology, 2 Linggong Road, Ganjingzi District, Dalian 116024, Liaoning, China. Email: liluyu@dlut.edu.cn

Abstract

The clutching inertia model is an ideal BangBang control model that is difficult to achieve in practice through passive control. In this paper, a single flywheel resettable-inertia damper (SRID) is proposed based on the clutching inertia device. This device is implemented with a rack-and-pinion system, a commutation and shift system, and an eddy current damping system with flywheel, which can create a vibration reduction effect in parallel with clutching inertia and damping. Initially, a simplified mechanical analysis model of this device is established. Subsequently, a comparative analysis of the control effects of SRID and viscous damper is conducted in a single-degree-of-freedom (SDOF) structures subjected to harmonic and seismic excitations. The results show that the SRID can achieve the same control effect as viscous damper with only a small damping coefficient, reflecting the role of clutching inertia. At the same time, according to the hysteresis curve, it also exhibits significant negative stiffness characteristics. The control device proposed in this paper can achieve a passive form of the BangBang control model to some extent, demonstrating promising application prospects.

Keywords: clutching inertia, eddy current damping, commutation and shift system, passive control

Introduction

With the emergency of inerter (Smith 2002),many inerter-based devices have been proposed and developed recently. Ikago et al. (2012) proposed a new control device called the tuned viscous mass damper (TVMD), which is reformed by a supplemental
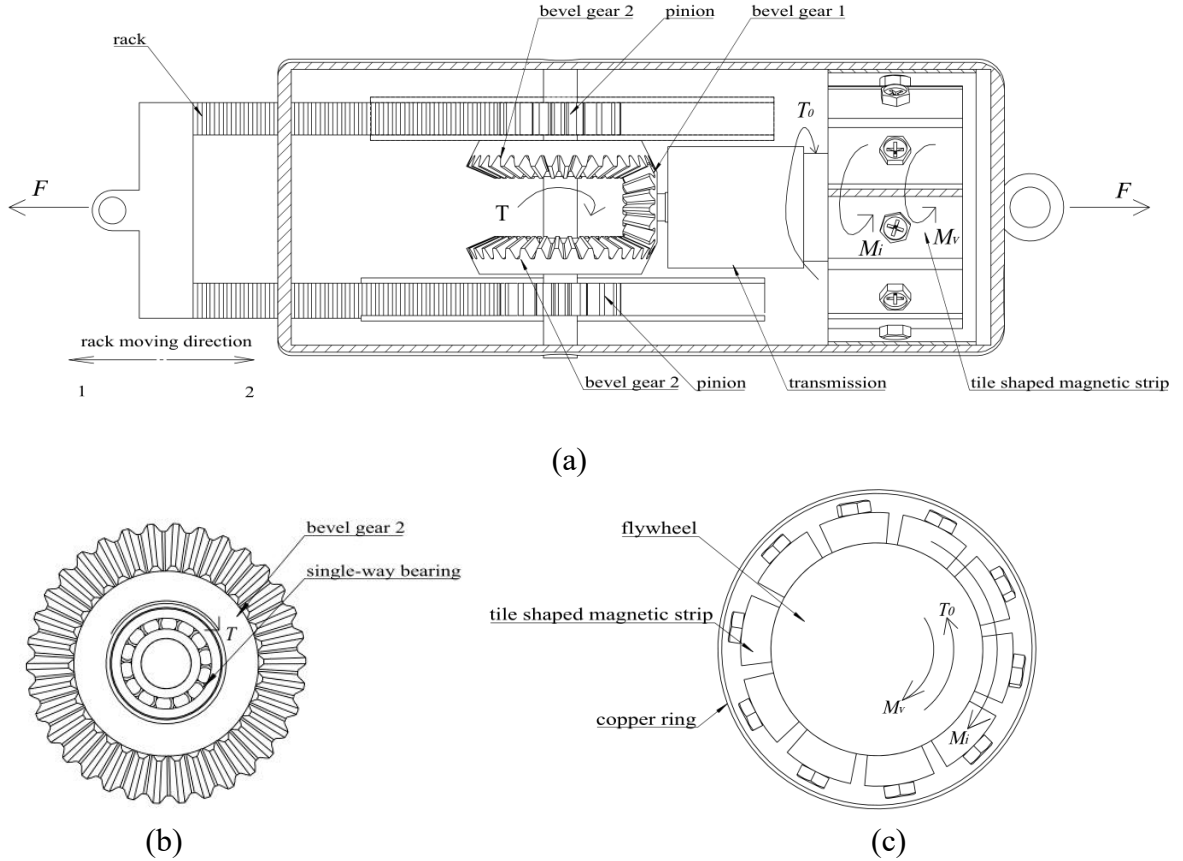
oscillator and the viscous mass damper (VMD). Gyro-mass device, essentially as an inertia device was proposed by Saitoh (2012) using for reducing large lateral displacements into the dynamic responses of base isolation systems. Lazar et al. (2014) proposed tuned inerter damper (TID) trying to replace tuned mass damper (TMD). By connecting the TMD in series with the inerter, a novel tuned mass-damper–inerter (TMDI) was proposed (Marian and Giaralis 2014), which can either replace part of the TMD vibrating mass to achieve lightweight passive vibration control solutions, or improve the performance of the classical TMD for a given TMD mass. Makris and Kampas (2016) proposed supplemental rotational inertia and concluded that the seismic protection of structures with supplemental rotational inertia has the unique advantage of suppressing the spectral displacements of long-period structures. The novel tuned mass damper with inerter which enables changes of inertance was proposed (Brzeski et al. 2017) ,which prove that the examined prototype of the TMD with the inerter and the CVT provides remarkable damping properties in a notably wide range of vibration frequencies. A new type of inerter with easily adjustable inertance and superior adaptability, called a crank train inerter (CTI), was investigated for structural vibration isolation(Tai et al. 2023), which could reduce the story drift ratio and deformation of the isolation layer.

In this study, we employ a single degree of freedom (SDOF) system incorporating a single flywheel resettable-inertia damper (SRID) to elucidate the characteristics of the device. First, configuration and components of the SRID was introduced in detail. Next, we establish the mechanical modeling of the SRID based on moment equilibrium for the SRID system at the preliminary design state. We compare the effectiveness of viscous damper (VD) and SRID by examining the controlled effects of the primary system subjected to harmonic and seismic excitation. Finally, conclusions are summarized to clarify the effectiveness of SRID on the structural response.

Configuration of the Novel Single Flywheel Resettable-Inertia Damper (SRID)
The single flywheel resettable-inertia damper (SRID) consists of a rack-and-pinion system, a commutation and shift system, and an eddy current damping system with flywheel as Fig. 1(a). This pair of bevel gears 2 has a clutching effect with a pair of single-way bearings (Fig. 1(b)). When the racks move along the direction 1 or 2, the pinions is driven, and then one side bevel gear 2 engages with the single-way bearing, driving the bevel gear 1 to rotate, and the other side bevel gear 2 engages with the follower, which means bevel gear 1 only could rotate in one direction because of the

single-way bearings, avoiding damage to the rack-and-pinion caused by reverse braking of the flywheel when the structure moves shiftly. The transmission is incorporated to accelerate the rotation of the flywheel, which in turn boosts the inertance of the device and generates eddy currents (Fig. 1(c)) and then dissipate energy. Additionally, the one-way rotation feature of the flywheel holds significant promise for energy collection within the device.

(a)

(b)   (c)

Fig. 1. Single flywheel resettable-inertia damper device: (a) vertical view; (b)bevel gear 2 with single-way bearing; and (c) eddy currents damping cross-section view.

Table I Notation

x	Displacement of the primary structure
$\dot{x}$	Velocity of the primary structure
$\ddot{x}$	Acceleration of the primary structure
m	Mass of the primary structure
c	Damping coefficient of the primary structure
k	Stiffness of the primary system
$\dot{\theta}_0$	Angular velocity of the flywheel
$\ddot{\theta}_0$	Angular acceleration of the flywheel
b_{max}	Maximum inertial mass of the device

c_{max}	Maximum damping coefficient of the device
F	Force transmitted by the device to the primary structure
m_0	Mass of the flywheel
J	Moment of inertia of the flywheel
r_0	The radius of flywheel
r_1	The radius of pinion
r_2	The radius of bevel gear 2
r_3	The radius of bevel gear 1
n	Gear ratio of the transmission
B	Magnetic induction intensity of tiled strips
R_m	The outer radius of the tiled magnetic strips
b_m	The width of the tiled magnetic strips
t	The thickness of the tiled magnetic strips
ρ	Electrical resistivity of the tiled magnetic strips
T_0	Torque applied to the flywheel input
M_i	Inertial torque of flywheel
M_v	Torque caused by rotating vicious liquid of internal tube

Dynamic Analysis of the SRID System

Mechanical Modeling of the SRID

At the preliminary design stage, for the mechanical analysis of the device, mechanical modeling of the SRID is established based on moment equilibrium, which torque applied to the flywheel T_0, inertial torque of flywheel M_i and torque caused by rotating to cut through magnetic induction lines M_v satisfy

$$T_0 = M_i + M_v \tag{1}$$

According to the transmission ratio of the gears, determine angular acceleration of the flywheel $\ddot{\theta}_0$

$$\ddot{\theta}_0 = n \frac{r_2}{r_1 r_3} \ddot{x} \tag{2}$$

where n is gear ratio of the transmission, $\ddot{x}$ acceleration of the primary structure, and r_1, r_2, r_3 are the radii of spur gear, bevel gear 2, bevel gear 1, respectively.

Because of the mass of the flywheel larger than that of other parts, the mass of other parts is ignored, the moment of inertia of the flywheel is

$$J = \frac{1}{2} m_0 r_0^2 \tag{3}$$

where J, m_0, r_0 are moment of inertia, mass and radius of the flywheel, respectively. Therefore, substituting Eqs. (2) and (3) in Eq. (4), we obtain inertial

torque of flywheel is

$$M_i = J\ddot{\theta}_0 = n\frac{r_2}{2r_1r_3}m_0r_0^2\ddot{x}. \tag{4}$$

Torque caused by rotation of internal tube M_v refer to (Chen et al., 2016)

$$M_v = F_B R_m = \frac{\pi B^2 b_m t R_m}{\rho}\dot{\theta}_0 r_0 \cdot R_m = \frac{\pi B^2 b_m t R_m^2}{\rho}\frac{nr_0r_2}{r_1r_3}\dot{x} \tag{5}$$

where B, b_m, t, R_m, ρ are magnetic induction intensity, width, thickness, outer radius and electrical resistivity of the tiled magnetic strips, respectively.

According to the mechanical principle, determine the torque of the flywheel

$$T_0 = \frac{1}{n}\frac{r_1r_3}{r_2}F \tag{6}$$

Substituting Eqs. (4), (5) and (6) in Eq. (1), the force F can be described as

$$F = \frac{n^2}{2}\left(\frac{r_0}{r_1}\right)^2\left(\frac{r_2}{r_3}\right)^2 m_0\ddot{x} + n^2\left(\frac{r_2}{r_1r_3}\right)^2\frac{\pi B^2 b_m t R_m^2 r_0}{\rho}\dot{x} \tag{7}$$

Therefore, we obtain maximum inertia-to-mass ratio b_{max} and maximum damping coefficient c_{max}

$$b_{max} = \frac{n^2}{2}\left(\frac{r_0}{r_1}\right)^2\left(\frac{r_2}{r_3}\right)^2 m_0 \tag{8}$$

$$c_{max} = \left(\frac{r_2}{r_1r_3}\right)^2\frac{\pi B^2 b_m t R_m^2 r_0}{\rho} \tag{9}$$

According to these, we could calculate rough approximation of the maximum parameters of the device to design based on the linear inerter without single-way bearings.
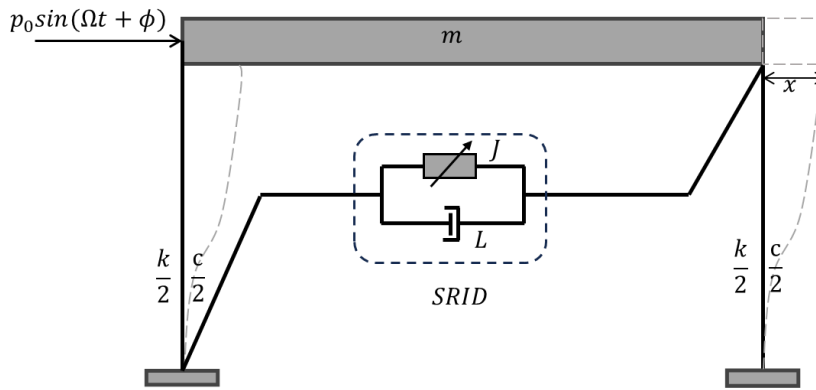
Modeling of Equation of Motion

First, based on the mechanical device, we simplify the structural device to the dynamic model established as Fig. 2. Then, the equation of motion about resettable clutching inerter damping system can be expressed as

$$\begin{cases} m\ddot{x} + c\dot{x} + kx + F = p_0\sin(\Omega t + \phi) \\ J\ddot{\theta}_0 + \mathrm{L}\dot{\theta}_0 = |T|\cdot n\frac{r_3}{r_2} \\ T = C_C\left(|\dot{\theta}_1| - \dot{\theta}_2\right)\frac{\left(sign(|\dot{\theta}_1| - \dot{\theta}_2) + 1\right)}{2}sign(\dot{\theta}_1) \\ F = \frac{T}{r_1}, \dot{\theta}_1 = \frac{\dot{x}}{r_1}, \dot{\theta}_2 = \frac{nr_3}{r_2}\dot{\theta}_0 \\ L = \frac{\pi B^2 b_m t R_m}{\rho}r_0^2 \end{cases} \tag{10}$$

where $x, \dot{x}, \ddot{x}$ are displacement, velocity, and acceleration of primary structure and $\dot{\theta}_0, \ddot{\theta}_0$ are angular velocity and angular acceleration of flywheel, respectively;

$\dot{\theta}_1, \dot{\theta}_2$ are angular velocities of single-way bearing and bevel gear 2,respectively; $J = \frac{1}{2}m_0 r_0^2, L$ are the moment of inertia and rotational damping coefficient of flywheel, respectively; r_0, r_1, r_2, r_3 are the radii of flywheel, pinion, bevel gear 1 and 2, respectively; F is the force output by the SRID on the primary structure; T is torque applied to single-way bearing; B, b_m, t, R_m, ρ are magnetic induction intensity, width, thickness, outer radius and electrical resistivity of the tiled magnetic strips, respectively; C_C is the damping coefficient of the connecting damping element between the single-way bearing and the bevel gear 2 (Liang and Li 2023).
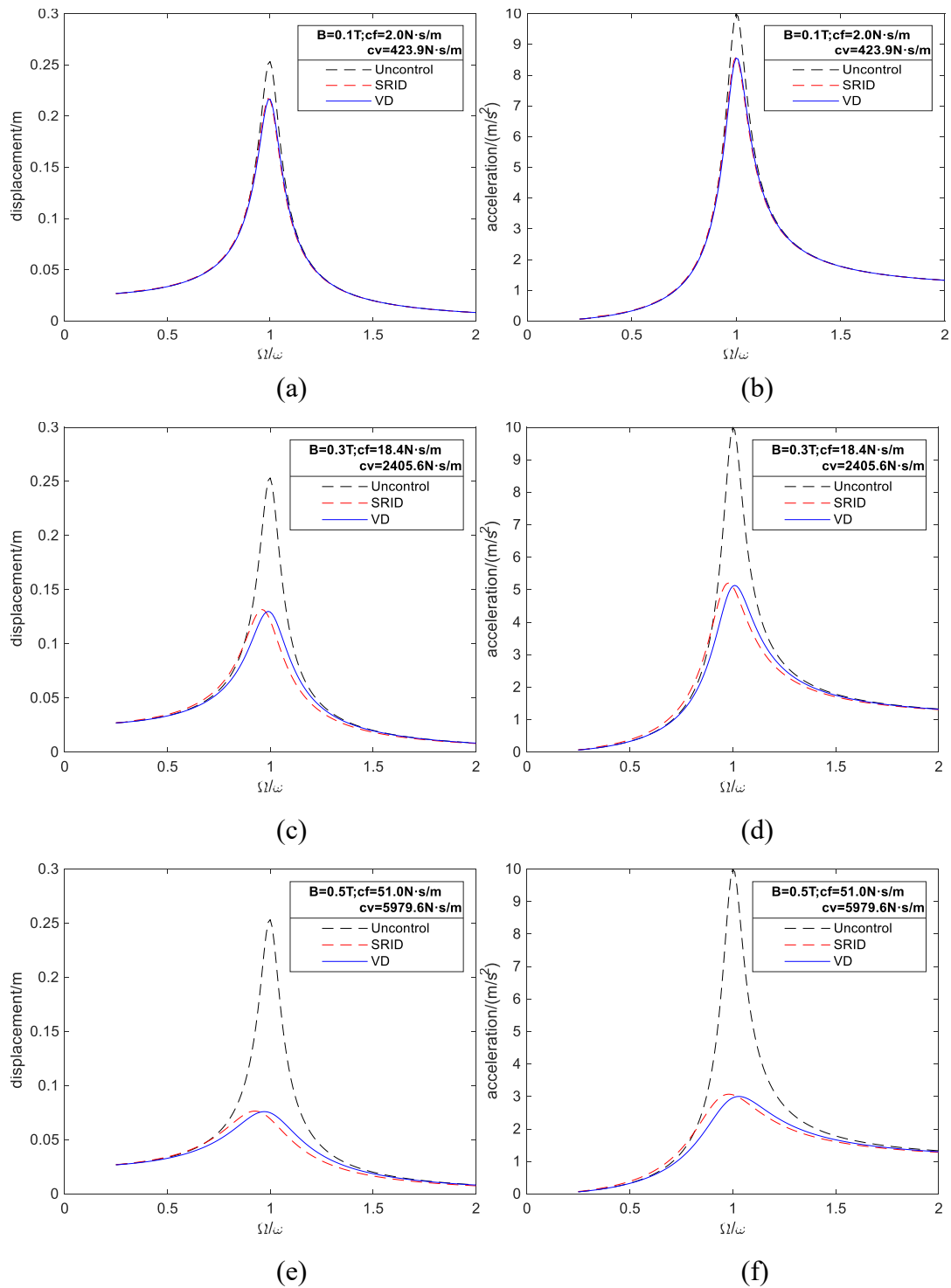

Fig. 2. Mechanical model for a SDOF with Single flywheel resettable-inertia damper (SRID).

Performance analysis of SRID subjected to harmonic excitation

Equivalent translational damping coefficient of the flywheel could be defined as

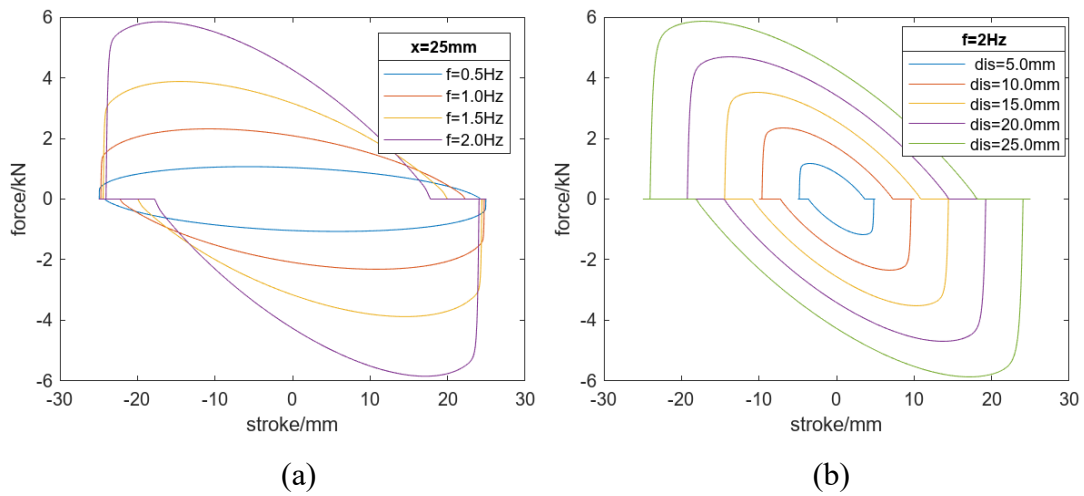$$c_f = \frac{L}{r_0^2} = \frac{\pi B^2 b_m t R_m}{\rho} \tag{11}$$

According to the same peak values of the frequency response curves of the viscous damping system and the SRID system with period of the primary structure =1s as Fig. 3, compare both of the damping coefficients and analyze the energy dissipation capacity about VD and SRID. When the peaks are nearly equal, the viscous damping coefficient is much larger than the damping coefficient of the flywheel of SRID. In other words, when the two damping coefficients are equal, the SRID system outperforms the VD system in terms of reducing displacement and acceleration.
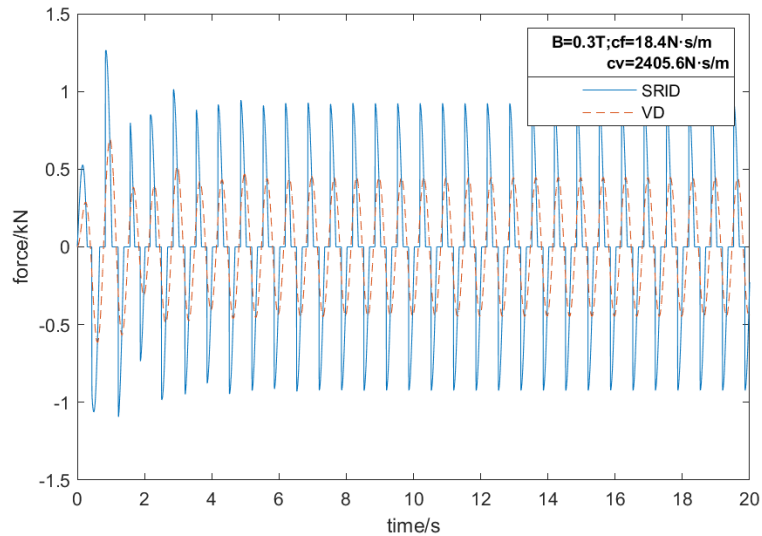
Fig. 3. Frequency response curves of the SRID, VD systems: (a), (c), (e) displacement; (b), (d), (f) acceleration when B=0.1,0.3,0.5T respectively. (The period of the primary structure is 1s.)

As depicted in Fig. 4, we observe that within a specific range of loading frequencies, there is a direct correlation between the loading frequency and the

output force of the device. In other words, as the loading frequency increases, the device generates a greater output force. Furthermore, within a designated displacement range of the primary structure, a larger primary structure displacement corresponds to a more pronounced output force from the device. This phenomenon underscores the negative stiffness characteristic of SRID, leading to more complete hysteresis loops and significant energy dissipation. Fig. 5 demonstrates that in the time history curve, the output force of SRID experiences multiple time intervals where it equals 0 kN. This observation reflects the role of one-way bearings and indicates the partial achievement of BangBang control.

(a)   (b)

Fig. 4. Hysteresis loops of (a) for f =0.5,1.0,1.5,2.0Hz when $x = 25mm$; and (b) displacement=5,10,15,20,25mm when f =2.0Hz.
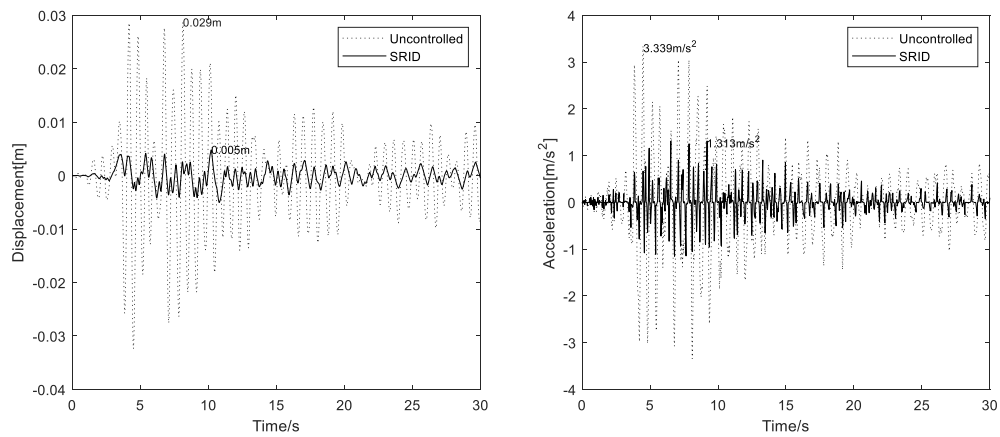

Fig. 5. The output forces of time history curves of SRID and VD in SDOF structures. (The period of the primary structure is 1s.)
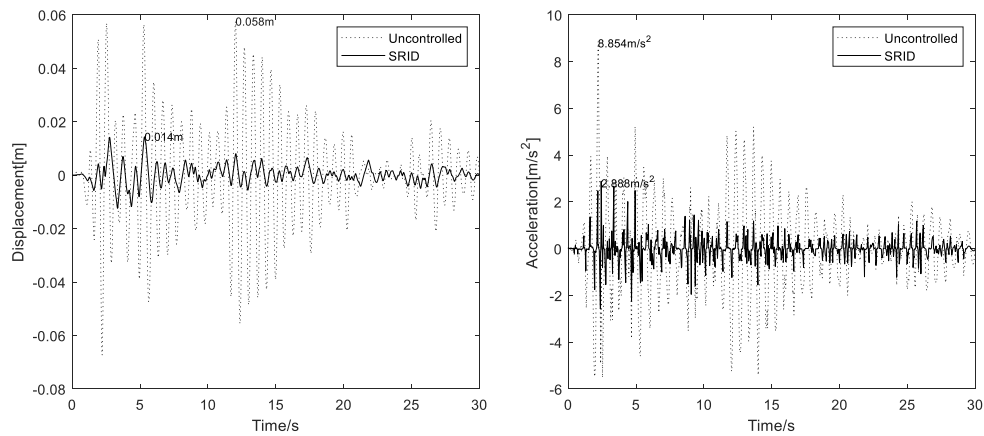
Performance analysis of SRID subjected to seismic excitation

Time-history analysis is implemented by numerical integration using MATLAB Simulink, with a time interval Δt of 0.001s. The observed earthquake records used for applying the ground acceleration $\ddot{u}_g$ to the models were as follows: (1) Taft EW (1952), (2) El Centro NS (1940), and (3) Tianjin NS (1976).
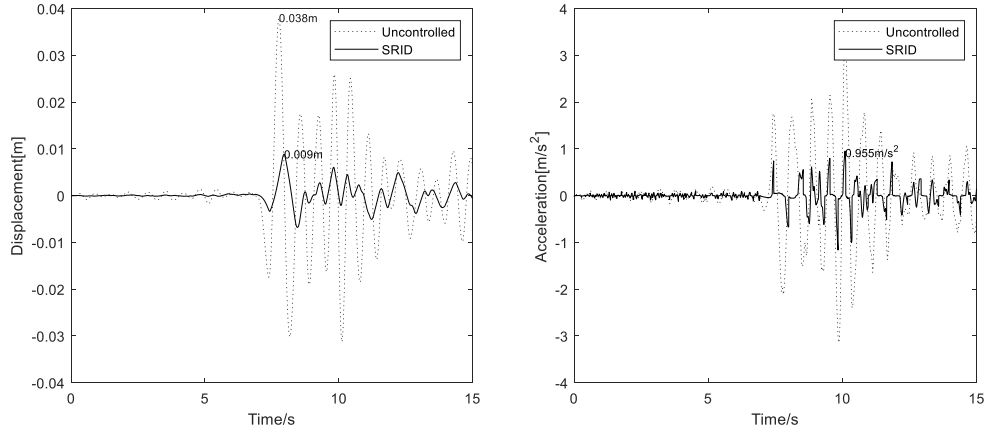
The time histories of the relative displacement with respect to the ground and the acceleration $\ddot{u}_g$ of the uncontrolled and SRID system are plotted for Taft EW, El Centro NS, and Tianjin NS (Fig. 6), where the responses of the models using the SRID device are compared with the responses of the uncontrolled system.
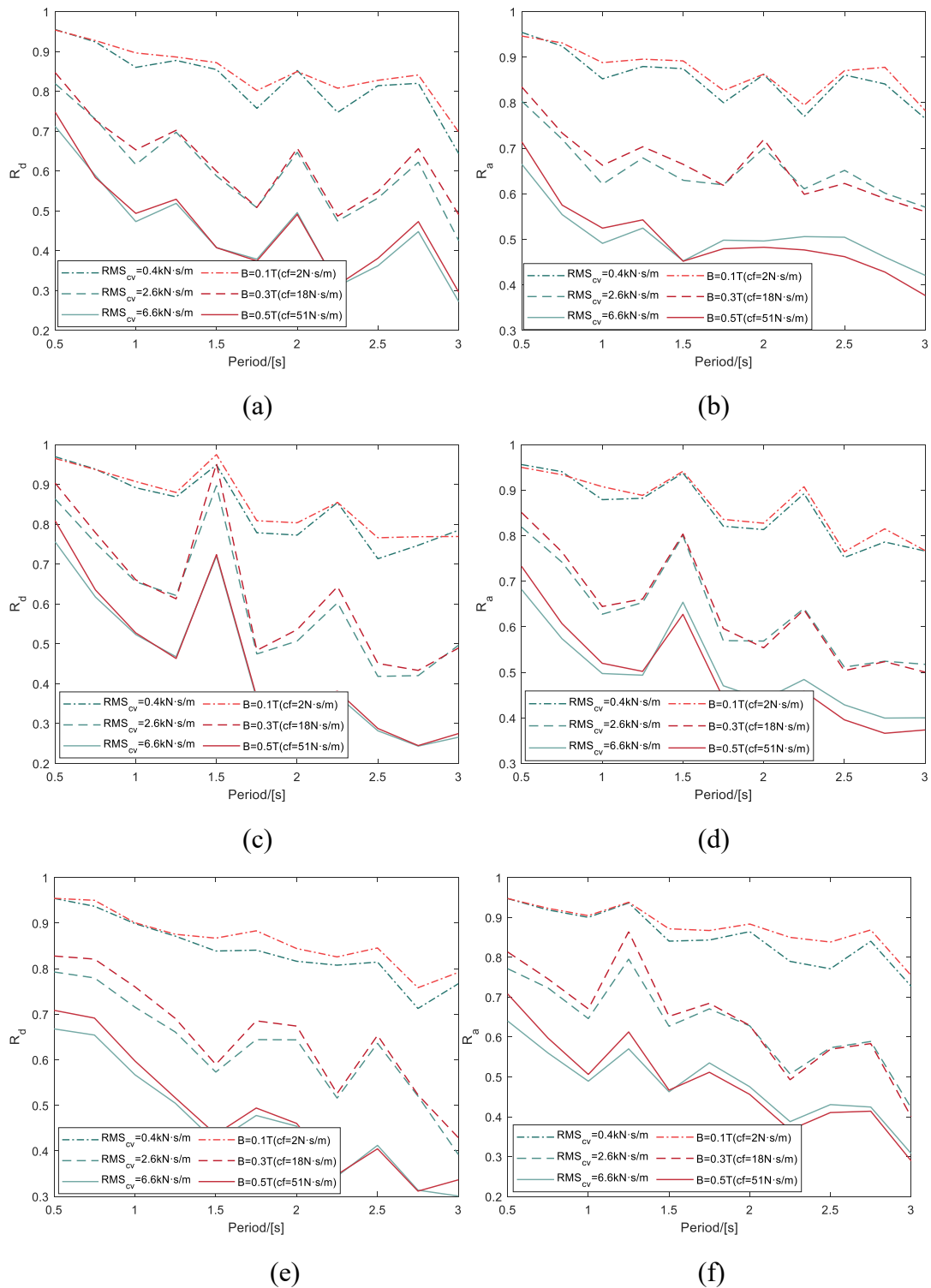

(a)

(b)

(c)

Fig. 6. Time-history responses of displacements (left) and response accelerations (right): comparison between uncontrolled system and SRID system excited by (a) Taft (1952) ;(b) El Centro (1940) ;(c) Tianjin (1976); the maximum amplitudes of responses were marked on the figure.

Otherwise, the uncontrolled, VD and SRID three systems are subjected to 20 artificial waves in different site conditions. The procedure for generating artificial excitations can be found in a previous study by Li and Liang (2020). The displacement and acceleration reduction effect is evaluated by the factor defined as follows:

$$R_d = \frac{D_{VD} \, or \, D_{SRID}}{D_{SDOF}}; R_a = \frac{A_{VD} \, or \, A_{SRID}}{A_{SDOF}} \qquad (12)$$

where D_{SDOF} and A_{SDOF}= mean peak displacement and acceleration response of the 5% damped primary structure; D_{SRID} and A_{SRID} = mean peak displacement and acceleration response of the SRID system; D_{VD} and A_{VD} = mean peak displacement and acceleration response of the VD system.

Fig. 7 shows the displacement and acceleration reduction effect of the VD and SRID systems varying with structural period and the damping coefficients. When the two systems can achieve the same reduction effect basically, the mean square value of the viscous damping coefficient is much larger than the damping coefficient of SRID, which means only need a small amount of damping control effect could be achieved with for SRID system, side embodies the effect of the inertia. These confirms the conclusion in the previous subsection.

Fig. 7. Reduction effect: (a), (c), (e) displacement and (b), (e), (f) acceleration; and (a), (b) soft soil; (c), (d)medium soil; (e), (f)firm soil. $\mathbf{RMS_{cv}}$ means the roots of square of the viscous damping coefficients with different primary structures.

Conclusion

In this study, we proposed a novel single flywheel resettable-inertia damper and explained its movement. We derived its maximum inertia and maximum damping coefficients. According to the equations of motion, numerical simulation results showed its better performance in harmonic excitation, which indicates that the device has very good negative stiffness and energy dissipation characteristics. Subjected to Taft (1952), El Centro (1940), Tianjin (1976) waves respectively, the displacement and acceleration responses of the SRID system were significantly reduced compared to the uncontrolled structure. The displacement and acceleration reduction effect about VD and SRID systems in different site conditions were calculated when inputting 20 artificial waves. When both damping coefficients equal, reduction effect of SRID system is more effective than VD system.

Reference

Brzeski, P., Lazarek, M., Perlikowski, P., 2017. Experimental study of the novel tuned mass damper with inerter which enables changes of inertance. Journal of Sound and Vibration 404, 47–57. https://doi.org/10.1016/j.jsv.2017.05.034

Chen, Z.-Q., Tian, J.-Y., Huang, Z.-W., Wang, J.-H., 2016. Calculation and test correction method of plane type eddy current damping coefficient. Zhongguo Gonglu Xuebao/China Journal of Highway and Transport 29, 46–53.

Ikago, K., Saito, K., Inoue, N., 2012. Seismic control of single-degree-of-freedom structure using tuned viscous mass damper. Earthquake Engineering & Structural Dynamics 41, 453–474. https://doi.org/10.1002/eqe.1138

Lazar, I.F., Neild, S. a., Wagg, D. j., 2014. Using an inerter-based device for structural vibration suppression. Earthquake Engineering & Structural Dynamics 43, 1129–1147. https://doi.org/10.1002/eqe.2390

Li, L., Liang, Q., 2020. Seismic Assessment and Optimal Design for Structures with Clutching Inerter Dampers. J. Eng. Mech. 146, 04020016. https://doi.org/10.1061/(ASCE)EM.1943-7889.0001732

Liang, Q., Li, L., 2023. Theoretical and experimental analyses of structures with supplemental clutching inertia devices. Earthquake Engineering & Structural Dynamics 52, 609–623. https://doi.org/10.1002/eqe.3776

Makris, N., Kampas, G., 2016. Seismic Protection of Structures with Supplemental Rotational Inertia. J. Eng. Mech. 142, 04016089.

https://doi.org/10.1061/(ASCE)EM.1943-7889.0001152

Marian, L., Giaralis, A., 2014. Optimal design of a novel tuned mass-damper–inerter (TMDI) passive vibration control configuration for stochastically support-excited structural systems. Probabilistic Engineering Mechanics 38, 156–164. https://doi.org/10.1016/j.probengmech.2014.03.007

Saitoh, M., 2012. On the performance of gyro-mass devices for displacement mitigation in base isolation systems. Structural Control and Health Monitoring 19, 246–259. https://doi.org/10.1002/stc.419

Smith, M.C., 2002. Synthesis of mechanical networks: the inerter. IEEE Transactions on Automatic Control 47,1648–1662. https://doi.org/10.1109/TAC.2002.803532

Tai, Y., Xu, Y., Hua, X., Chen, C., Wang, W., Chen, Z., 2023. A New Type of Inerter with Easily Adjustable Inertance and Superior Adaptability: Crank Train Inerter. Journal of Structural Engineering 149, 04023063. https://doi.org/10.1061/JSENDH.STENG-12154